Nature of itinerant ferromagnetism of $SrRuO_3$: A DFT+DMFT study

Minjae Kim and B. I. Min

Department of Physics, PCTP, Pohang University of Science and Technology, Pohang 790-784, Korea

(Received 12 February 2015; revised manuscript received 20 April 2015; published 18 May 2015)

We have investigated the temperature-dependent evolution of electronic structures and magnetic properties of an itinerant ferromagnet $SrRuO_3$, employing the combined scheme of density functional theory and dynamical mean-field theory (DFT+DMFT). The inclusion of finite dynamical correlation effects beyond DFT well describes not only the incoherent hump structure observed in the photoemission experiment but also the temperature-dependent magnetic properties in accordance with experiments. We have shown that the magnetization of $SrRuO_3$ evolves with the Stoner behavior below the Curie temperature T_c, reflecting the weak itinerant ferromagnetic behavior, but the local residual magnetic moment persists even above T_c, indicating the local magnetic moment behavior. We suggest that the ferromagnetism of $SrRuO_3$ has a dual nature of both weak and local moment limits, even though the magnetism of $SrRuO_3$ is more itinerant than that of Fe.

DOI: 10.1103/PhysRevB.91.205116 PACS number(s): 75.30.−m, 71.15.Mb, 71.20.−b

I. INTRODUCTION

Electronic correlation effects in itinerant ferromagnetism are one of the most essential subjects in condensed-matter physics [1]. In general, there are two limits in describing itinerant ferromagnetism. One is the weak ferromagnetic limit, in which the magnetic behavior below the Curie temperature T_c is well described by the Stoner theory. In this limit, the correlation effect is not very strong, and the Curie-Weiss susceptibility above T_c is explained by the spin fluctuation in the reciprocal space. The other is the local moment limit, in which the magnetic behavior is well described by the Heisenberg theory. The Curie-Weiss susceptibility above T_c is explained by the localized spin in real space. For example, $ZrZn_2$ is thought to be close to the weak ferromagnetic limit [2], while Fe is close to the local moment limit [3]. Many itinerant ferromagnets, however, seem to be in the intermediate regime between those two limits. Usually, both longitudinal and transverse spin fluctuations have been taken into account to describe itinerant ferromagnets in the intermediate regime [4,5].

$SrRuO_3$ is a well-known itinerant ferromagnet which has numerous interesting properties [6]. The fundamental question on $SrRuO_3$ is whether its magnetism belongs to the weak ferromagnetic limit or to the local moment limit. Low-temperature electronic structures and magnetic properties of $SrRuO_3$ are well described by band structure calculations based on the standard density functional theory (DFT) [7–9]. However, there are also several experimental indications of the sizable electronic correlation effects and the localized magnetic moment in real space. Photoemission (PES) data show that there is an incoherent hump spectrum at 1 eV below the Fermi level E_F, which is a signature of the non-negligible electronic correlation strength U [10,11]. According to magneto-optical and angle-resolved photoemission spectroscopy (ARPES) experiments, there remains a finite exchange splitting up to T_c (∼160 K), reflecting the local magnetic moment behavior [12,13]. Indeed, the ratio of the Curie-Weiss moment and the saturation moment, P_c/P_s, is close to 1 (∼1.3), implying the existence of local magnetic moment [14]. The temperature T derivative of the magnetic part of the resistivity also shows the local magnetic moment above T_c [15]. According to recent T-dependent optical data [16], the magnetic moment below T_c evolves with Stoner behavior, but above T_c, there is a finite short-range-ordered localized magnetic moment that drops linearly with increasing T.

These experimental indications suggest that, to describe the itinerant ferromagnetism of $SrRuO_3$, one may have to take into account the dual nature of Ru 4d electrons, itinerancy, and localization. The DFT+U method considering the static electronic correlation U was used to describe the incoherent hump feature in PES experiments [17]. DFT+U, however, cannot describe both the coherent and incoherent spectra simultaneously. In view of the dual nature of Ru 4d electrons in $SrRuO_3$, the electronic correlation effect should be included dynamically. Thus, the combination of DFT and the dynamical mean-field theory (DFT+DMFT) will be a good choice for the realistic description of the electronic structure of $SrRuO_3$ [18]. Actually, both the coherent and incoherent structures in the PES of Ru 4d bands were reported to be well described by the DMFT [19]. However, the important T-dependent evolution of electronic structures and magnetic properties of $SrRuO_3$ has not been explored yet and is the subject of the present study.

We have shown that the inclusion of the dynamical correlation effect of Ru 4d electrons in $SrRuO_3$ successfully describes not only its correlated electronic structure but also the T-dependent evolution of electronic structure and magnetism in accordance with experiments. We have confirmed that, below T_c, the magnetic moment evolves with the Stoner behavior, reflecting the itinerant ferromagnetism. In addition, we have shown that there is a localized magnetic moment, which remains even above T_c and diminishes linearly upon heating.

II. COMPUTATIONAL METHODS

We have performed the DFT+DMFT calculations based on the projection-embedding scheme, as implemented in Ref. [20]. The correlated Ru 4d electrons were treated dynamically with the DMFT local self-energy with t_{2g} and e_g orbital projections, while the s and p electrons were treated on the DFT level. The DFT calculation was done using the full-potential linearized augmented plane wave (FLAPW) band method [21,22]. As an impurity solver, we used the continuous-time quantum Monte Carlo method and performed

the analytical continuation [20,23,24]. For Coulomb interaction parameters, U and J, we have employed $U = 3$ eV and $J = 0.6$ eV, as in existing DMFT calculations [19], which describe experimental results of $SrRuO_3$ well [17,25–28]. We used the density-density form of the local Coulomb interaction in the DMFT impurity solver for computational efficiency. We have also performed the spin-polarized DFT calculations to compare the DFT and DFT+DMFT results. For the crystal structure of $SrRuO_3$, we have adopted the experimental structure of the orthorhombic *Pnma* space group [29]. We give more computational details and the crystal structures in Appendix A.

III. RESULTS AND DISCUSSION

Figure 1 presents the band structures obtained with the DFT and DFT+DMFT schemes at $T = 100$ K. In fact, the DFT+DMFT results represent the spectral functions $A(k,\omega)$. The seemingly complicated band structures of Ru t_{2g} and e_g arise from the band folding from the cubic to the orthorhombic Brillouin Zone (BZ). This feature is consistent with a recent report for a similar ruthenate, $CaRuO_3$, which has the same *Pnma* space group [30]. There are interesting differences between DFT and DFT+DMFT. In DFT+DMFT, one can notice the following: (i) the narrowing of the coherent band near E_F, (ii) the emergence of the incoherent feature below E_F, especially for the spin-up band, and (iii) the reduction of the exchange splitting. These features arise from the electronic correlation effects and have also been observed in the previous DFT+DMFT calculations for Fe and Ni [31].

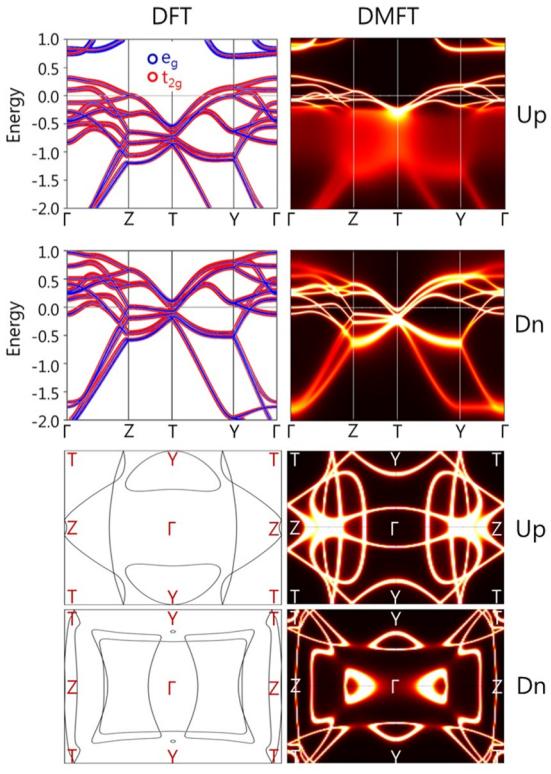

FIG. 1. (Color online) (top) Band structures obtained with DFT (left) and DFT+DMFT at $T = 100$ K (right). The size of the red (blue) dot in the DFT plot denotes the amount of the t_{2g} (e_g) component in the wave function. (bottom) DFT FSs (left) and DFT+DMFT FSs at $T = 100$ K (right). Up and Dn denote spin up and down, respectively. The first BZ is provided in Appendix A.

The flat bands in the vicinity of E_F in Fig. 1 are the Ru t_{2g} bands. It is seen that, due to the correlation effects, the DFT+DMFT spin-up (majority spin) bands below -0.3 eV become mostly incoherent, and those above -0.3 eV that are coherent become narrowed with respect to the corresponding DFT bands. In contrast, the DFT+DMFT spin-down bands show just overall band narrowing and a weak incoherent feature near the top. The more incoherent feature in the spin-up band than in the spin-down band has already been seen in previous experimental and theoretical studies on itinerant ferromagnets, such as Fe, Co, and Ni [31–33]. Due to almost filled spin-up t_{2g} bands, the electron-hole pair scatterer is composed of mainly spin-down electrons. The stronger Coulomb scattering between spin-up and -down electrons will produce larger self-energy for the spin-up electrons, which brings about the more incoherent feature in the spin-up band. It is also notable that, in DFT+DMFT, the spin-up and -down bands are shifted slightly up and down, respectively, so the exchange splitting becomes smaller than that in DFT.

In the bottom panel of Fig. 1, Fermi surfaces (FSs) obtained with the DFT and DFT+DMFT schemes are provided. Seemingly different FSs between DFT and DFT+DMFT arise from the smaller exchange splitting in DFT+DMFT. In DFT+DMFT spin-up FSs, due to the shifting up of the bands, electron pockets become smaller, hole pockets become larger, and new hole pockets emerge compared to those in DFT. For example, the electron pocket at $k = T$ becomes smaller, the hole pocket at $k = Z$ becomes larger, and new hole pockets appear between Γ and Z. Just the opposite situation occurs for the DFT+DMFT spin-down FSs due to the shifting down of the bands. For example, the electron pocket between Γ and Y becomes larger, the hole pocket between Γ and Z becomes smaller, and new electron pockets appear at $k = T$.

Comparing the DFT+DMFT results in Fig. 1 to ARPES data provides valuable information on the correlation effects. The spin-up hole pocket FS at $k = Z$ is much larger in DFT+DMFT than in DFT. The large hole pocket at $k = Z$ is indeed observed in the ARPES experiment [13]. As shown in Appendix A, the orbital character of this hole pocket at $k = Z$ is xy and yz, which is consistent with the analysis of the ARPES experiment [13,34,35]. On the other hand, ARPES shows a kink feature in the spectral function at 65 meV below E_F along Γ and Z [13]. This kink was considered to arise from the electron-boson interaction, which was proposed as an origin of the small quasiparticle weight, $Z \sim 0.3$. However, in our DFT+DMFT results, there is no clear kink feature near E_F, and the obtained Z's below T_c are 0.63 and 0.88 for the spin-up and -down bands, respectively [see Fig. 4(d)], which are much larger than the experimental $Z \sim 0.3$ [36]. Our results for Z are consistent with previous DFT+DMFT results [37]. This indicates that the kink near E_F and the additional quasiparticle renormalization might not originate from the local electron-electron interaction but from another electron-boson interaction, such as a phonon or q-dependent magnon that requires a scheme beyond the single-site DMFT.

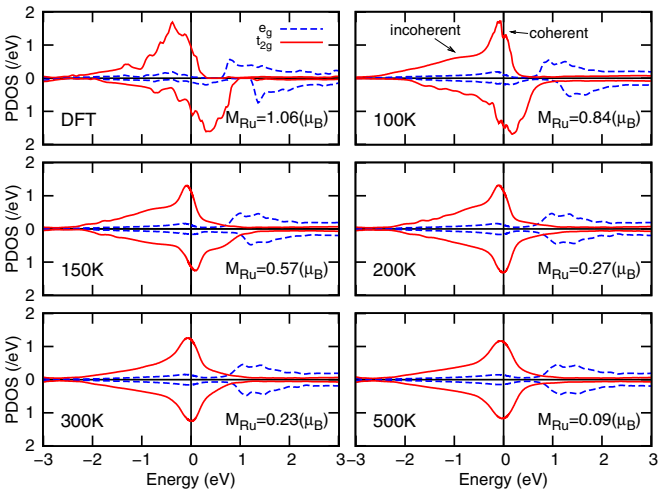

FIG. 2. (Color online) Ru 4d partial density of states (PDOS) from DFT and DFT+DMFT at different T. Red solid and blue dashed lines represent t_{2g} and e_g projected PDOSs, respectively. Calculated magnetic moment M_{Ru} at each T is provided. For DFT+DMFT at $T = 100$ K, the coherent and incoherent parts are indicated.

Figure 2 presents the partial densities of states (PDOSs) of t_{2g} and e_g orbitals of Ru 4d electrons in the DFT and DFT+DMFT schemes. The PDOSs manifest the low-spin state of Ru 4d electrons with small occupancy of the e_g orbital. Note that the exchange splitting in DFT+DMFT decreases upon heating. Interestingly, there still remains a finite exchange splitting near T_c ($T \sim 150$ K), which is consistent with magneto-optical [12] and ARPES experiments [13].

To examine the signature of electronic correlation effects in $SrRuO_3$, the Ru 4d PES spectrum [10,17] is compared with near-E_F PDOSs of DFT and DFT+DMFT ($T = 100$ K) in Fig. 3. Different from the DFT PDOS, the DFT+DMFT PDOS shows both the coherent and the incoherent parts and the shallow dip structure in between, which is consistent with

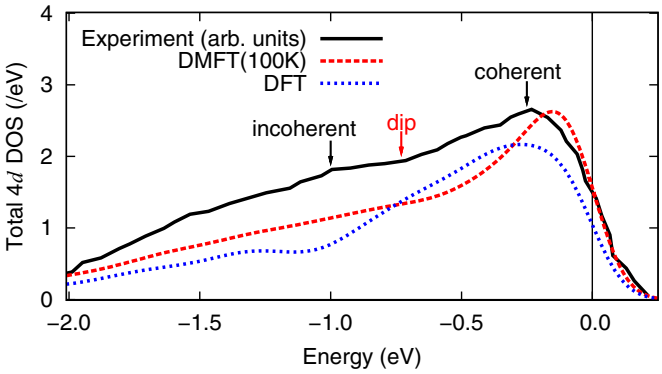

FIG. 3. (Color online) The Ru 4d PES spectrum (black solid line) [10,17] is compared with the calculated PDOSs in DFT and DFT+DMFT (100 K). Blue dotted and red dashed lines represent the DFT and DFT+DMFT PDOSs, respectively, which are broadened with a Gaussian function (0.10 eV FWHM). The coherent part at -0.25 eV, the dip at -0.73 eV, and the incoherent part at -1 eV in the PES data are indicated.

the experimental PES data. Interestingly, the peak position of the incoherent PDOS, 1 eV below E_F, is in agreement with that in the previous DFT+U ($U = 1$ eV) result [17]. The consistency between the DFT+U and DFT+DMFT results justifies the use of a bit larger $U = 3$ eV in DMFT [28].

The finite dynamical Coulomb correlation in DFT+DMFT also reproduces the correct T-dependent magnetic properties of $SrRuO_3$. Figure 4(a) presents the DFT+DMFT results of the Ru magnetic moment M_{Ru} in $SrRuO_3$ versus T, which shows that there are two regimes for the evolution of M_{Ru} with increasing T. Below $T = 200$ K, M_{Ru} drops rather rapidly upon heating. On the other hand, above $T = 200$ K, M_{Ru} diminishes rather slowly upon heating. It is noteworthy that a significant local magnetic moment remains near T_c ($0.27\mu_B$ at $T = 150$ K), which seems to persist even above T_c. According to the Stoner theory, the local magnetic moment at $T = 0$ is supposed to be close to the DFT value ($1.06\mu_B$), and it drops to zero at T_c with the T^2 scaling behavior, as represented by the blue line in Fig. 4(a). Thus the M_{Ru}-T curve in Fig. 4(a) indicates that the Stoner theory of itinerant magnetism is not appropriate for describing the T-dependent evolution of the local magnetic moment in $SrRuO_3$ above T_c. It is seen that the T-dependent behavior is different below and above $T = 200$ K. We designate the T regimes below and above $T = 200$ K as the Stoner and residual moment regimes, respectively.

Figures 4(b) and 4(c) present T-dependent behaviors of magnetic moment in the Stoner and the residual moment regimes, respectively. In the Stoner regime below T_c, Fig. 4(b) clearly shows that the magnetic moment diminishes with the T^2 scaling, which is in good agreement with the T-dependent spectrum evolution in the optical experiment [16]. On the other hand, in the residual moment regime in Fig. 4(c), the finite local magnetic moment above T_c is seen to diminish linearly with T, which is again consistent with the optical spectrum experiment [16]. The T-dependent exchange splitting Δ_{ex} of the t_{2g} band in the inset of Fig. 4(a) also follows the T^2 and T scaling behaviors below and above T_c, respectively. The disappearance of the net macroscopic magnetic moment above T_c would be driven by the long-wavelength transversal spin-wave excitations of the persistent local residual moment [16,31].

The linearly diminishing behavior of the local magnetic moment above T_c in $SrRuO_3$ is reminiscent of the theoretically suggested behavior in Fe, which was derived by using the Monte Carlo simulation including both longitudinal and transverse spin fluctuations [5]. This kind of simulation is in line with the intermediate approach between the weak ferromagnetic limit and the local moment limit. However, in the case of $SrRuO_3$, our result shows that the persistent local moment above T_c is smaller and diminishes more rapidly with increasing T than in Fe. For Fe, the persistent local moment above T_c is close to the $T = 0$ value with very little reduction because Fe is close to the local moment limit. This difference indicates that the magnetic properties of $SrRuO_3$ are much more itinerant than those of Fe.

We have confirmed that ferromagnetic ordering restores the coherent metallic nature in $SrRuO_3$, as expected for a

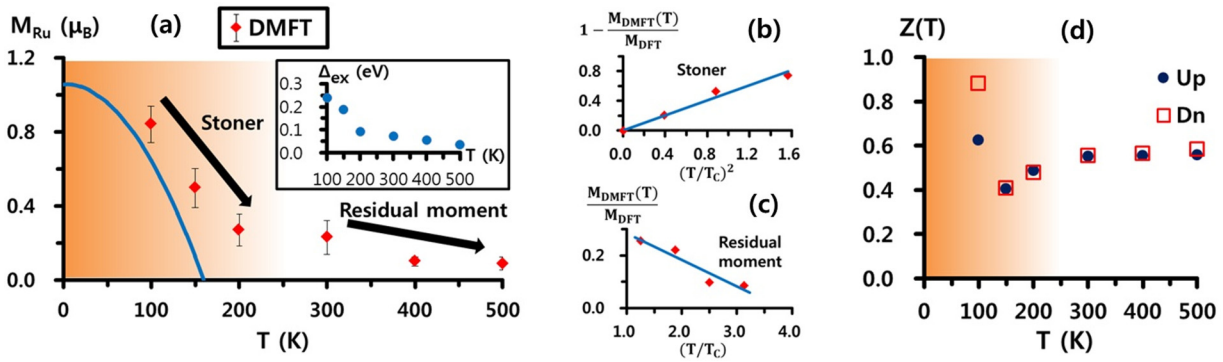

FIG. 4. (Color online) (a) The DFT+DMFT results for the Ru magnetic moment M_{Ru} in $SrRuO_3$ vs T. The blue line represents $M_{Ru}(T)$ with the Stoner behavior below $T_c = 160$ K [$M_{Ru}(0) = 1.06\mu_B$ from the DFT]. We assign the Stoner regime for $T < 200$ K and the residual moment regime for $T > 200$ K. In the former, $M_{Ru}(T)$ shows the fast drop with T, while in the latter, it shows the slow drop. We used averaged M_{Ru} values from the DMFT iterations, and the error bar corresponds to the standard deviation from the averaged value. The inset presents the T-dependent exchange splitting Δ_{ex} between spin-up and -down bands, which shows behavior similar to $M_{Ru}(T)$. Δ_{ex} is defined as a splitting between peak positions of spin-up and -down parts in the t_{2g} PDOS. (b) The reduction of the scaled magnetic moment of DFT+DMFT ($1 - \frac{M_{\rm DMFT}}{M_{\rm DFT}}$) vs the square of scaled temperature [$(T/T_c)^2$] in the Stoner regime. The blue linear line is from the least-squares fitting of data, including the origin. We employed $M_{\rm DFT}$ as $M_{Ru}(T = 0)$ since the experimental magnetic moment of $SrRuO_3$ is in good agreement with that in DFT [9,14]. (c) The scaled magnetic moment of the DFT+DMFT ($\frac{M_{\rm DMFT}}{M_{\rm DFT}}$) vs the scaled temperature (T/T_c) in the residual moment regime. The blue linear line is from the least-squares fitting. (d) The DFT+DMFT results for the quasiparticle weight Z of t_{2g} orbital vs T. Blue circles and red squares represent Z's for spin-up and -down electrons, respectively.

Hund's metal [38,39]. Figure 4(d) presents the T-dependent quasiparticle weight Z of the t_{2g} orbital. Z is estimated from the analytically continued self-energy of the t_{2g} orbital in DFT+DMFT ($Z = [1 - \frac{\partial}{\partial\omega}{\rm Re}\Sigma(\omega)]^{-1}\,|_{\omega=0}$). Above T_c ($\sim$150 K), the increasing spin-flip scattering upon cooling reduces the coherence of the t_{2g} orbital, as shown in the diminishing Z in Fig. 4(d). On the other hand, below T_c, the spin-flip scattering is suppressed with ferromagnetic ordering, as shown in the enhancement of Z upon cooling. Therefore, the crossover occurs near T_c from the spin-flip-induced incoherent regime to the ferromagnetic-ordering-induced coherent regime. We provide real frequency self-energies for several T's in Appendix B.

As mentioned earlier, for computational efficiency, we used the density-density form of the local Coulomb interaction instead of the rotationally invariant form. Thus the spin-flip scattering effect might be somewhat underestimated in the present calculations, and accordingly, the restoration of coherence might also be underestimated with the onset of ferromagnetism. The underestimation of the spin-flip scattering effect might also yield the overestimated T_c with respect to the experimental value. However, as shown in Ref. [40], the overestimation of T_c would be much smaller for systems close to the weak ferromagnetic limit, such as $SrRuO_3$ and Ni, than for those close to the local moment limit, such as Fe. Therefore more studies are required to clarify the effects of the rotationally invariant form of the Coulomb interaction for various itinerant ferromagnets.

IV. CONCLUSION

We have shown that the DFT+DMFT calculations describe correctly the correlated electronic structure and the T-dependent evolutions of local electronic structure and magnetic moment in $SrRuO_3$. The obtained Stoner behavior below T_c and the persistent local magnetic moment above T_c are consistent with experiments. The T-dependent local magnetic moment evolution in $SrRuO_3$ is similar to the case in Fe. A more rapid drop of local magnetic moment in $SrRuO_3$ above T_c, however, indicates that Ru $4d$ electrons in $SrRuO_3$ are more itinerant than Fe $3d$ electrons. The present study of the T-dependent electronic structures and magnetic properties based on the DFT+DMFT method will provide an important tool for understanding fundamental properties in various itinerant ferromagnets.

ACKNOWLEDGMENTS

Helpful discussions with C.-J. Kang, K. Kim, and B. H. Kim are greatly appreciated. This work was supported by the POSTECH BK21+ Physics Project, the Max-Plank POSTECH/KOREA Research Initiative, and the KISTI supercomputing center (Grant No. KSC-2014-C3-040).

APPENDIX A: COMPUTATIONAL DETAILS AND ORBITAL CHARACTERS OF BANDS

In the DFT part of the DFT+DMFT calculation, the local-density approximation (LDA) was used for the exchange and correlation functionals [41]. We used 1000 k points for the BZ sampling. In order to simulate the T-dependent ferromagnetism of $SrRuO_3$, we broke the symmetry between spin up and down in the self-energy. For the double-counting correction, we used the fully localized limit (FLL) formula with the fixed $4d$ electron occupancy from the LDA ($n_d = 5.32$). The FLL yields only a small energy difference from the around mean field (AMF) formula in the present case (0.0768 eV). We have also checked that our choice of $U = 3$ eV and $J = 0.6$ eV produces a reasonable magnetic moment of

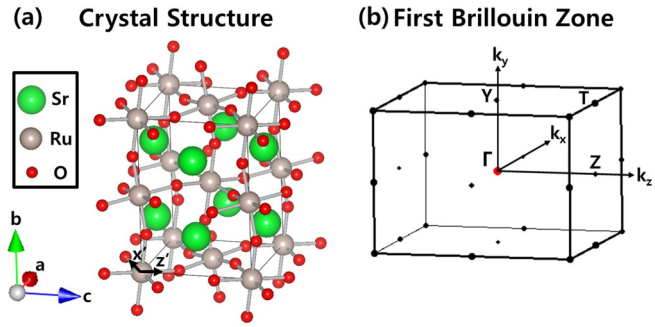

FIG. 5. (Color online) (a) The crystal structure of $SrRuO_3$. The local axes (x' and z'), which are used for the orbital projection in Fig. 7, are depicted. The y' axis is nearly parallel to the b axis. We have adopted the experimental structure of the *Pnma* space group [29]. (b) The first BZ of $SrRuO_3$. High-symmetry points Γ, Z, T, and Y for the band structure plots are depicted.

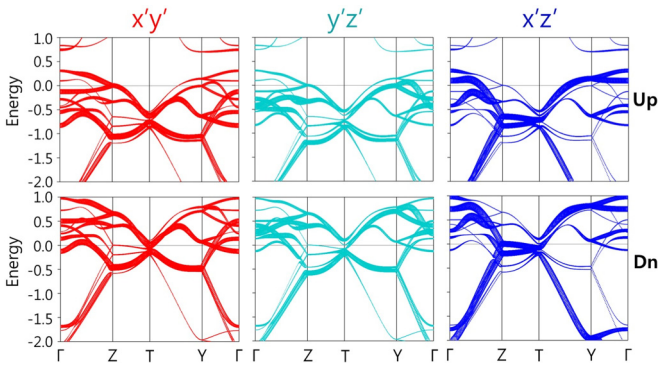

FIG. 6. (Color online) The orbital-projected DFT band structures of $SrRuO_3$. The size of the red, green, and blue dots denotes the amount of the $x'y'$, $y'z'$, and $x'z'$ components in the wave function, respectively. Up and Dn denote spin-up and -down bands. Note that the spin-up band at the Z point near E_F has $x'y'$ and $y'z'$ orbital characters.

Ru at 100 K for the FLL case, while for the AMF case, the U value should be larger than 3 eV but smaller than 4 eV to get a reasonable result.

In the DFT+DMFT calculation, we considered hybridization functions with an energy window of 20 eV around the Fermi level including both correlated t_{2g} and e_g orbitals. In Ref. [39], physically relevant parameters, $U = 2.3$ eV and $J = 0.32$ eV, were suggested for the frontier t_{2g} orbitals in the DFT+DMFT calculation of $SrRuO_3$. These parameters result in Hund's metallic nature in the ruthenium perovskites [39]. We think that our Coulomb interaction parameters, $U = 3.0$ eV and $J = 0.6$ eV, are compatible with the above parameters because of the wider energy window of the hybridization function. Indeed, we have checked that, if we use a smaller U of 1 or 2 eV, the Ru magnetic moment is found to be too small ($\sim 0.05\mu_B$).

We have used the charge non-self-consistent DFT+DMFT scheme because the combination of the spin-polarized DFT and DMFT has not been completely implemented yet. If we perform the charge self-consistent DFT+DMFT calculation with the non-spin-polarized DFT loop, the itinerant ferromagnetism of $SrRuO_3$ would not be treated properly because the spin dependence in the hybridization function from DMFT would be distorted in the non-spin-polarized DFT loop.

To reduce orbitally nondiagonal components of the hybridization function in the DFT+DMFT, we used the local axes presented in Fig. 5(a). The orbital-projected DFT band structures are provided in Fig. 6 along the symmetry lines shown in Fig. 5(b).

To reduce the statistical noise from the continuous-time quantum Monte Carlo method, we averaged each five-step self-energy in consecutive order from 31 to 80 DMFT iterations to obtain eight analytically continued self-energies [20]. Then we averaged magnetic moments from these eight self-energies at each T and chose the electronic structure of the one that had the magnetic moment closest to the averaged value.

APPENDIX B: SELF-ENERGY

The self-energies of $SrRuO_3$ in DFT+DMFT are provided in Fig. 7. The reduction of exchange splitting with increasing T is evident in the $\mathrm{Re}\Sigma(\omega = 0)$. The trend of the $\frac{\partial \mathrm{Re}\Sigma(\omega)}{\partial \omega}|_{\omega=0}$ value with variation of T is consistent with that of Z. Upon cooling, the $-\frac{\partial \mathrm{Re}\Sigma(\omega)}{\partial \omega}|_{\omega=0}$ value first increases with the enhancement spin-flip scattering, and with the onset of ferromagnetism at $T = 100$ K, the $-\frac{\partial \mathrm{Re}\Sigma(\omega)}{\partial \omega}|_{\omega=0}$ value decreases due to the reduction of spin-flip scattering.

The signature of the Fermi-liquid behavior is apparent in the low-energy part (0.2 eV around E_F) at 100 K, as displayed by the ω linear behavior in $\mathrm{Re}\Sigma(\omega)$ and the ω square behavior in $\mathrm{Im}\Sigma(\omega)$. The deviation from the Fermi-liquid behavior in the higher-energy part is similar to that in $CaRuO_3$ [30].

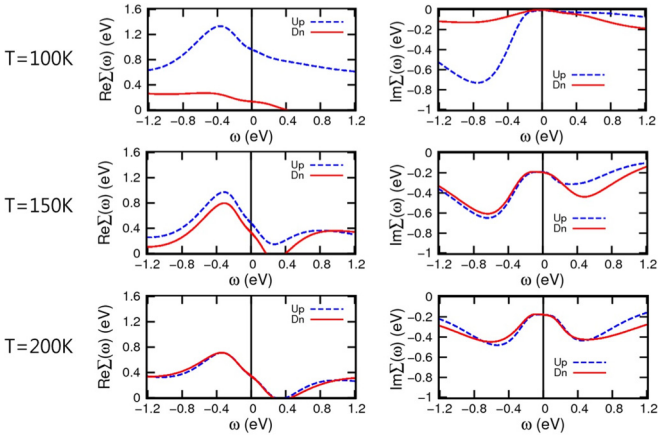

FIG. 7. (Color online) The self-energies of $SrRuO_3$ in DFT+DMFT for $T = 100$, 150, and 200 K (top, middle, and bottom). Left (right) panels are for real (imaginary) self-energies. Blue dashed (red solid) lines present spin up (spin down).

[1] T. Moriya, *Spin Fluctuations in Itinerant Electron Magnetism* (Springer, Berlin, 1985).

[2] E. P. Wohlfarth, J. Appl. Phys. **39**, 1061 (1968).

[3] M. Uhl and J. Kübler, Phys. Rev. Lett. **77**, 334 (1996).

[4] V. Korenman, J. L. Murray, and R. E. Prange, Phys. Rev. B **16**, 4032 (1977).

[5] A. V. Ruban, S. Khmelevskyi, P. Mohn, and B. Johansson, Phys. Rev. B **75**, 054402 (2007).

[6] G. Koster, L. Klein, W. Siemons, G. Rijnders, J. S. Dodge, C.-B. Eom, D. H. A. Blank, and M. R. Beasley, Rev. Mod. Phys. **84**, 253 (2012).

[7] I. I. Mazin and D. J. Singh, Phys. Rev. B **56**, 2556 (1997).

[8] K. Fujioka, J. Okamoto, T. Mizokawa, A. Fujimori, I. Hase, M. Abbate, H. J. Lin, C. T. Chen, Y. Takeda, and M. Takano, Phys. Rev. B **56**, 6380 (1997).

[9] C. Etz, I. V. Maznichenko, D. Böttcher, J. Henk, A. N. Yaresko, W. Hergert, I. I. Mazin, I. Mertig, and A. Ernst, Phys. Rev. B **86**, 064441 (2012).

[10] D. Toyota, I. Ohkubo, H. Kumigashira, M. Oshima, T. Ohnishi, M. Lippmaa, M. Takizawa, A. Fujimori, K. Ono, M. Kawasaki, and H. Koinuma, Appl. Phys. Lett. **87**, 162508 (2005).

[11] M. Takizawa, D. Toyota, H. Wadati, A. Chikamatsu, H. Kumigashira, A. Fujimori, M. Oshima, Z. Fang, M. Lippmaa, M. Kawasaki, and H. Koinuma, Phys. Rev. B **72**, 060404(R) (2005).

[12] J. S. Dodge, E. Kulatov, L. Klein, C. H. Ahn, J. W. Reiner, L. Miéville, T. H. Geballe, M. R. Beasley, A. Kapitulnik, H. Ohta, Y. Uspenskii, and S. Halilov, Phys. Rev. B **60**, R6987(R) (1999).

[13] D. E. Shai, C. Adamo, D. W. Shen, C. M. Brooks, J. W. Harter, E. J. Monkman, B. Burganov, D. G. Schlom, and K. M. Shen, Phys. Rev. Lett. **110**, 087004 (2013).

[14] A. Kanbayasi, J. Phys. Soc. Jpn. **41**, 1876 (1976).

[15] L. Klein, J. S. Dodge, C. H. Ahn, J. W. Reiner, L. Mieville, T. H. Geballe, M. R. Beasley, and A. Kapitulnik, J. Phys. Condens. Matter **8**, 10111 (1996).

[16] D. W. Jeong, H. C. Choi, C. H. Kim, S. H. Chang, C. H. Sohn, H. J. Park, T. D. Kang, D.-Y. Cho, S. H. Baek, C. B. Eom, J. H. Shim, J. Yu, K. W. Kim, S. J. Moon, and T. W. Noh, Phys. Rev. Lett. **110**, 247202 (2013).

[17] J. M. Rondinelli, N. M. Caffrey, S. Sanvito, and N. A. Spaldin, Phys. Rev. B **78**, 155107 (2008).

[18] G. Kotliar, S. Y. Savrasov, K. Haule, V. S. Oudovenko, O. Parcollet, and C. A. Marianetti, Rev. Mod. Phys. **78**, 865 (2006).

[19] E. Jakobi, S. Kanungo, S. Sarkar, S. Schmitt, and T. Saha-Dasgupta, Phys. Rev. B **83**, 041103(R) (2011).

[20] K. Haule, C.-H. Yee, and K. Kim, Phys. Rev. B **81**, 195107 (2010).

[21] M. Weinert, E. Wimmer, and A. J. Freeman, Phys. Rev. B **26**, 4571 (1982).

[22] P. Blaha, K. Schwarz, G. Madsen, D. Kvasnicka, and J. Luitz, WIEN2K (Karlheinz Schwarz, Techn. Universität Wien, Austria, 2001).

[23] K. Haule, Phys. Rev. B **75**, 155113 (2007).

[24] P. Werner, A. Comanac, L. de' Medici, M. Troyer, and A. J. Millis, Phys. Rev. Lett. **97**, 076405 (2006).

[25] J. S. Ahn, J. Bak, H. S. Choi, T. W. Noh, J. E. Han, Y. Bang, J. H. Cho, and Q. X. Jia, Phys. Rev. Lett. **82**, 5321 (1999).

[26] H.-D. Kim, H.-J. Noh, K. H. Kim, and S.-J. Oh, Phys. Rev. Lett. **93**, 126404 (2004).

[27] B. Kim and B. I. Min, Phys. Rev. B **89**, 195411 (2014).

[28] The U value of 3 eV is apparently somewhat larger than that used in the DFT+U method ($\sim$1 eV) [17,27]. The reason for using larger U in DMFT is that the given bare U is to be reduced by the screening channel in the DMFT impurity solver.

[29] C. W. Jones, P. D. Battle, P. Lightfoot, and W. T. Harrison, Acta Crystallogr., Sect. C **45**, 365 (1989).

[30] H. T. Dang, J. Mravlje, A. Georges, and A. J. Millis, arXiv:1412.7803.

[31] A. I. Lichtenstein, M. I. Katsnelson, and G. Kotliar, Phys. Rev. Lett. **87**, 067205 (2001).

[32] S. Monastra, F. Manghi, C. A. Rozzi, C. Arcangeli, E. Wetli, H.-J. Neff, T. Greber, and J. Osterwalder, Phys. Rev. Lett. **88**, 236402 (2002).

[33] A. Grechnev, I. Di Marco, M. I. Katsnelson, A. I. Lichtenstein, J. Wills, and O. Eriksson, Phys. Rev. B **76**, 035107 (2007).

[34] The y axis in the *Pnma* space group is the z axis in the *Pbnm* space group, which is the [001] axis of the $SrRuO_3$ film on the substrate [13].

[35] The film thickness in the ARPES measurement [13] is about 50 monolayers, which is close to the bulk limit [10]. Thus we compared our bulk DFT+DMFT results with ARPES results from Ref. [13].

[36] P. B. Allen, H. Berger, O. Chauvet, L. Forro, T. Jarlborg, A. Junod, B. Revaz, and G. Santi, Phys. Rev. B **53**, 4393 (1996).

[37] O. Grånäs, I. Di Marco, O. Eriksson, L. Nordström, and C. Etz, Phys. Rev. B **90**, 165130 (2014).

[38] A. Georges, L. de'Medici, and J. Mravlje, Annu. Rev. Condens. Matter Phys. **4**, 137 (2013).

[39] H. T. Dang, J. Mravlje, A. Georges, and A. J. Millis, arXiv:1501.03964 [Phys. Rev. B (to be published)].

[40] A. S. Belozerov, I. Leonov, and V. I. Anisimov, Phys. Rev. B **87**, 125138 (2013).

[41] J. P. Perdew and Y. Wang, Phys. Rev. B **45**, 13244 (1992).